

Thermodynamic Discovery of Tetracriticality and Emergent Multicomponent Superconductivity in UTe_2

Sahas Kamat,¹ Jared Dans,² Shanta Saha,² Artem D. Kokovin,³
Johnpierre Paglione,^{2,4} Jörg Schmalian,^{3,5} and B. J. Ramshaw^{1,4,*}

¹Laboratory of Atomic and Solid State Physics, Cornell University, Ithaca, NY 14853, USA

²Maryland Quantum Materials Center, Department of Physics,
University of Maryland, College Park, Maryland 20742, USA

³Institute for Theory of Condensed Matter, Karlsruhe Institute of Technology, Karlsruhe 76131, Germany

⁴Canadian Institute for Advanced Research, Toronto, Ontario, Canada

⁵Institute for Quantum Materials and Technologies,

Karlsruhe Institute of Technology, Karlsruhe 76131, Germany

(Dated: March 19, 2026)

The candidate topological superconductor UTe_2 exhibits a complex phase diagram with multiple superconducting states, yet the nature of their coexistence has remained a central mystery. In particular, the apparent intersection of two second-order phase boundaries at a “triple point” in the pressure-temperature phase diagram is thermodynamically forbidden, suggesting hidden phase transitions or a fundamental misunderstanding of the superconductivity in UTe_2 . Here, we use pulse-echo ultrasound to resolve this puzzle by discovering a new phase boundary that is characterized by a unique “upward jump” in the sound velocity—direct thermodynamic evidence for a re-entrant phase transition. Our results establish (P^*, T^*) as a tetracritical point, beyond which the ambient and pressure-induced superconducting order parameters form a multi-component state. We use the measured phase diagram to construct a Ginzburg-Landau theory that shows that strong competition between the two superconducting order parameters drives the re-entrance and leads to phase locking that suppress superconducting fluctuations. These findings provide the definitive magnetic field-temperature-pressure phase diagram and establish a thermodynamic foundation for multi-component—and potentially topological—superconductivity in UTe_2 .

INTRODUCTION

Multi-component superconductivity occurs when two (or more) order parameters condense at the same time: the most famous example—once thought to be the superconducting state of Sr_2RuO_4 [1]—is the chiral $p_x + ip_y$ state in ^3He [2]. Multi-component order parameters are a frequent ingredient for a topological superconductor [3, 4], but to date there are very few—if any—confirmed examples outside of ^3He .

UTe_2 currently stands as the most viable candidate for spin-triplet, multi-component superconductivity. While it is generally agreed that the zero-field, ambient-pressure state (SC1) is single-component [5, 6] there is clear evidence for a distinct superconducting state (SC2) that emerges under hydrostatic pressure [7–10]. Whether these phases coexist in some region of the pressure-temperature phase diagram and form a multi-component state—one that is potentially topological—is currently unknown.

The central challenge is the presence of an enigmatic multicritical point at (P^*, T^*) in the pressure-temperature phase diagram, where the SC2 critical-temperature line terminates on the SC1 line (indicated

by a star in Figure 1). Specific-heat [7] and magnetization [9] measurements clearly indicate that all transitions are second order and occur in the bulk. However, a “triple point” of second-order phase transitions, shown in Fig. 1(b), is thermodynamically forbidden [11], whereas the additional second-order line required for a tetracritical point, shown in Fig. 1(a), has remained elusive. Attempts to resolve this puzzle have led to speculations ranging from a hidden phase boundary [7–10], to a fine-tuned superconducting transition with a vanishing specific-heat jump [7, 10], and even to the possibility of a third-order phase transition [9].

Resolving these issues has implications that go beyond simply determining the topology of the UTe_2 phase diagram: for example, the continuation of the SC2 phase boundary past the critical point, as sketched in Figure 1a, implies a region where the order parameters of SC1 and SC2 are simultaneously finite and with the potential for topological superconductivity.

In this work, we use pulse-echo ultrasound to map out the full field-pressure-temperature (B - P - T) phase diagram of UTe_2 in the vicinity of the critical pressure P^* , where the two transitions meet. We find that the SC2 phase boundary extends past the SC1 phase boundary, leading to a region of two-component order SC1+SC2 in the phase diagram. We demonstrate that SC1 and SC2 interact strongly in this regime, with novel re-entrance behavior of the SC1 phase at temperatures

* bradramshaw@cornell.edu

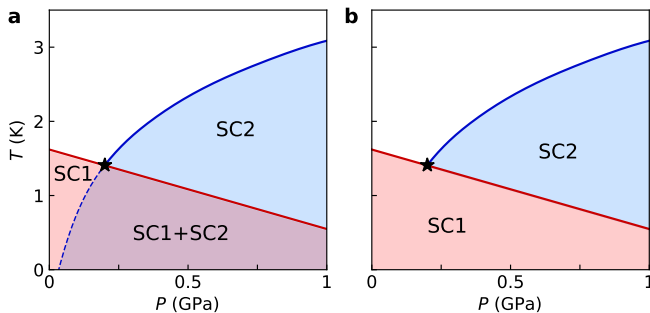


FIG. 1. **Proposed temperature-pressure phase diagrams for UTe_2 .** The elusive multicritical point is indicated by a black star. The well-established SC1 and SC2 phase boundaries are shown as solid red and blue lines respectively. a) A proposed phase diagram where the SC2 phase boundary extends past the critical point, with a region of co-existence of the SC1 and SC2 phases (shaded purple). Such a scenario implies the existence of a phase boundary indicated with a blue dashed line—this boundary has not yet been observed. b) In a second proposal, the SC2 phase boundary terminates upon meeting the SC1 phase boundary. Given the weak heat capacity anomalies, this requires a third-order superconducting transition, where second derivatives of the free energy (such as heat capacity) remain continuous [7, 11].

below the SC1+SC2 phase. We construct a phenomenological Ginzburg-Landau (GL) theory that accurately reproduces the observed phase diagram, and draw inferences from the constraints that our data place on the GL parameters and hence on the microscopic theory of superconductivity in UTe_2 . Finally, we explore the magnetic field dependence of this phase diagram and construct a coherent picture of the field-induced and pressure-induced superconducting states.

EXPERIMENT

Elastic moduli are thermodynamic coefficients: they are the second derivatives of a system’s free energy with respect to strain. In this way, they are similar to the specific heat—the second derivative of the free energy with respect to temperature. Like specific heat, we expect non-analyticity in the elastic moduli at a phase transition. Unlike specific heat—where there is only one coefficient—we expect different behaviour for the different elastic moduli depending on how they couple to the order parameter [12]. Generically, we expect “jumps” (discontinuities in elastic moduli) when the coupling is linear in strain, quadratic in order parameter, and “kinks” (discontinuities in the temperature derivatives of the elastic moduli) when the coupling is quadratic in strain, quadratic in order parameter.

Previous ultrasound measurements on UTe_2 have demonstrated that the ambient and pressure-induced superconducting states couple strongly to the c_{33} (compression)

and c_{55} (shear) moduli [5, 13]. We make simultaneous measurements of both c_{33} and c_{55} as a function of temperature at fixed pressures between $P = 0.11$ and $P = 0.77$ GPa, focusing on pressures near the critical point at $P^* = 0.20$ GPa (see Figure 1). Full experimental details are given in Kamat *et al.* [13].

RESULTS

Elastic Moduli in Zero Magnetic Field

Measurements of the c_{55} shear elastic modulus at different pressures and in zero magnetic field are shown in Figure 2b. At the two lowest pressures—0.11 GPa and 0.19 GPa—the transition to the SC1 state appears as a kink in c_{55} at T_{c1} . At pressures greater than P^* , two sharp kinks appear at two transitions whose separation in temperature increases with increasing pressure. Based on previous measurements of the phase diagram [7, 10, 13], we identify the upper and lower transitions as T_{c2} and T_{c1} , respectively.

Simultaneous measurements of the compression modulus c_{33} are shown in Figure 2c. For the two lowest pressures, c_{33} jumps downward at T_{c1} . At pressures greater than P^* , jumps appear at both T_{c1} and T_{c2} : the jump at T_{c2} grows larger with increasing pressure, whereas the jump at T_{c1} is only visible in the inset to Figure 2c. At $P = 0.21$ GPa—a pressure slightly greater than the critical pressure P^* —we measure an additional feature in c_{33} : an upward jump of equal magnitude to the downward jump at T_{c2} . The temperature at which this upward jump occurs does not correspond to either T_{c1} or T_{c2} , and we refer to it as T_{c2}^* .

We use the thermodynamic signatures in the elastic moduli at T_{c1} and T_{c2} to construct the phase diagram shown in Figure 2a. These phase boundaries are consistent with previous work [7–10, 13]. For reasons we will justify in the remainder of this manuscript, we place the T_{c2}^* point on a phase boundary connected to T_{c2} at the critical pressure P^* . This T_{c2}^* phase boundary has not been reported previously, and is the primary discovery of this work.

Temperature Reentrant SC2

The phase diagram in Figure 2a suggests a remarkable phenomenon: at $P = 0.21$ GPa, when decreasing the temperature from above the upper transition (T_{c2}), UTe_2 first enters the SC2 phase at T_{c2} , then enters a mixed SC1+SC2 phase at T_{c1} , then *loses* the SC2 component of the order parameter cooling through T_{c2}^* . While the kinks and jumps in the elastic moduli identify the locations of these phase transitions, we have not yet justified the assignment of T_{c2}^* to a phase boundary that connects to T_{c2} , nor have we justified the label “SC1+SC2”.

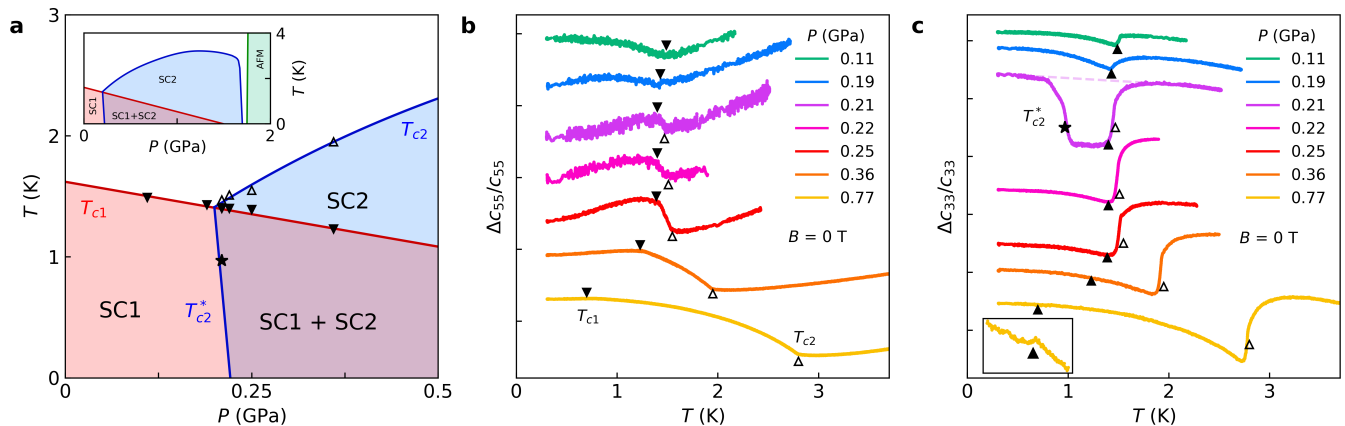


FIG. 2. **The phase diagram of UTe₂ near the tetracritical point.** a) The zero-field phase diagram of UTe₂ constructed in this work. T_{c1} , T_{c2} and T_{c2}^* are represented by solid triangles, hollow triangles, and a star respectively. The solid red and blue lines are guides to the eye that represent the SC1 and SC2 phase boundaries, respectively. Regions in phase space where the SC1 and SC2 order parameters are non-zero are shaded red and blue, respectively. Inset: The UTe₂ phase diagram over a larger pressure range, with T_{c1} and T_{c2} lines adapted from Braithwaite et al. [7] b) The c_{55} elastic modulus versus temperature in UTe₂ at different pressures. For $P < 0.2$ GPa, we find a single, sharp kink at T_{c1} . At $P > 0.2$ GPa, we find sharp kinks at both T_{c2} and T_{c1} . c) The c_{33} elastic modulus, measured simultaneously with the c_{55} elastic modulus. For $P < 0.2$ GPa, we find a downward jump at T_{c1} when UTe₂ enters the SC1 state. This jump grows for $P > 0.2$ GPa, and occurs at T_{c2} . At $P = 0.21$ GPa, we find an upward jump at T_{c2}^* as the sample exits the SC2 superconducting state upon cooling. Inset: The jump at T_{c1} at 0.77 GPa. The data shown are from a different sample optimized for a c_{33} measurement. We show quantitative similarity between both samples in the SI.

Second-order phase transitions are defined by discontinuities in certain derivatives of the free energy [14]. The most familiar example is the specific heat, $C/T = -\partial^2 F/\partial T^2$. Typically, this jump must be *upwards* on cooling through T_c as the system enters the ordered state. In a superconductor, opening a gap restricts the electronic degrees of freedom [15], causing the entropy decrease more rapidly below T_c than in the normal state and producing the characteristic upward jump. For a phase boundary like T_{c2}^* , however, the heat capacity must jump *downwards*—a behavior generally required at a back-bent phase transition line (see Methods). This has immediate implications for the elastic moduli.

Like the specific heat, elastic moduli are second derivatives of the free energy: $c_{ijkl} = \partial^2 F/\partial \epsilon_{ij} \partial \epsilon_{kl}$. For compression strains (such as ϵ_{zz}), the jumps in compression elastic moduli are related to the jump in the specific heat through an Ehrenfest relation. For $c_{33} \equiv c_{zzzz}$, the relationship is

$$\Delta c_{33} = -\frac{\Delta C}{T_c} \left(\frac{\partial T_c}{\partial \epsilon_{zz}} \right)^2. \quad (1)$$

The coefficient $(\partial T_c/\partial \epsilon_{zz})$ —the slope of T_c as a function of strain—always enters as the square, which means that Δc_{33} always has the opposite sign of ΔC . Conventionally, this means that the jump in a compression modulus at T_c must be *downwards*—a fact that is demonstrated at T_{c1} and T_{c2} in Figure 2c, and which has been documented for many other phase transitions [16].

At $P = 0.21$ GPa, c_{33} first jumps downward upon cool-

ing to $T_{c2} = 1.4$ K. Then, at $T_{c2}^* = 0.9$ K, c_{33} jumps *upwards*. By Equation 1, this requires that the specific heat jumps *downwards*, as required for a system that has *lost* order upon cooling. This is our primary evidence that T_{c2}^* marks the transition where the SC2 order parameter is lost upon cooling. We observe no hysteresis at T_{c2}^* when warming and cooling through the transition, demonstrating that this transition is second order (see Extended Data).

Having demonstrated that T_{c2}^* corresponds to a second order phase transition where order is lost upon cooling, we assign it to the second branch of the SC1 phase boundary. This boundary is nearly vertical in the $P - T$ phase diagram (Figure 2a). This assignment is consistent with the fact that the jump upwards at T_{c2}^* is equal to the jump downwards at T_{c2} —roughly speaking, the entropy lost upon entering the SC2 phase at T_{c2} is regained when exiting that phase at T_{c2}^* . It is worth noting that there is a second feature in c_{33} roughly 50 mK below T_{c2}^* . We attribute this to either small internal inhomogeneities or small external pressure inhomogeneities in the sample: because T_{c2}^* drops by nearly 1.5 K over a 0.01 GPa pressure range, even part-per-thousand inhomogeneities in the pressure can lead to smearing of T_{c2}^* over tens of mK.

Elastic moduli in a magnetic field

The T_{c2}^* phase boundary in Figure 2a is constrained by just a single data point. This is because T_{c2}^* exists only

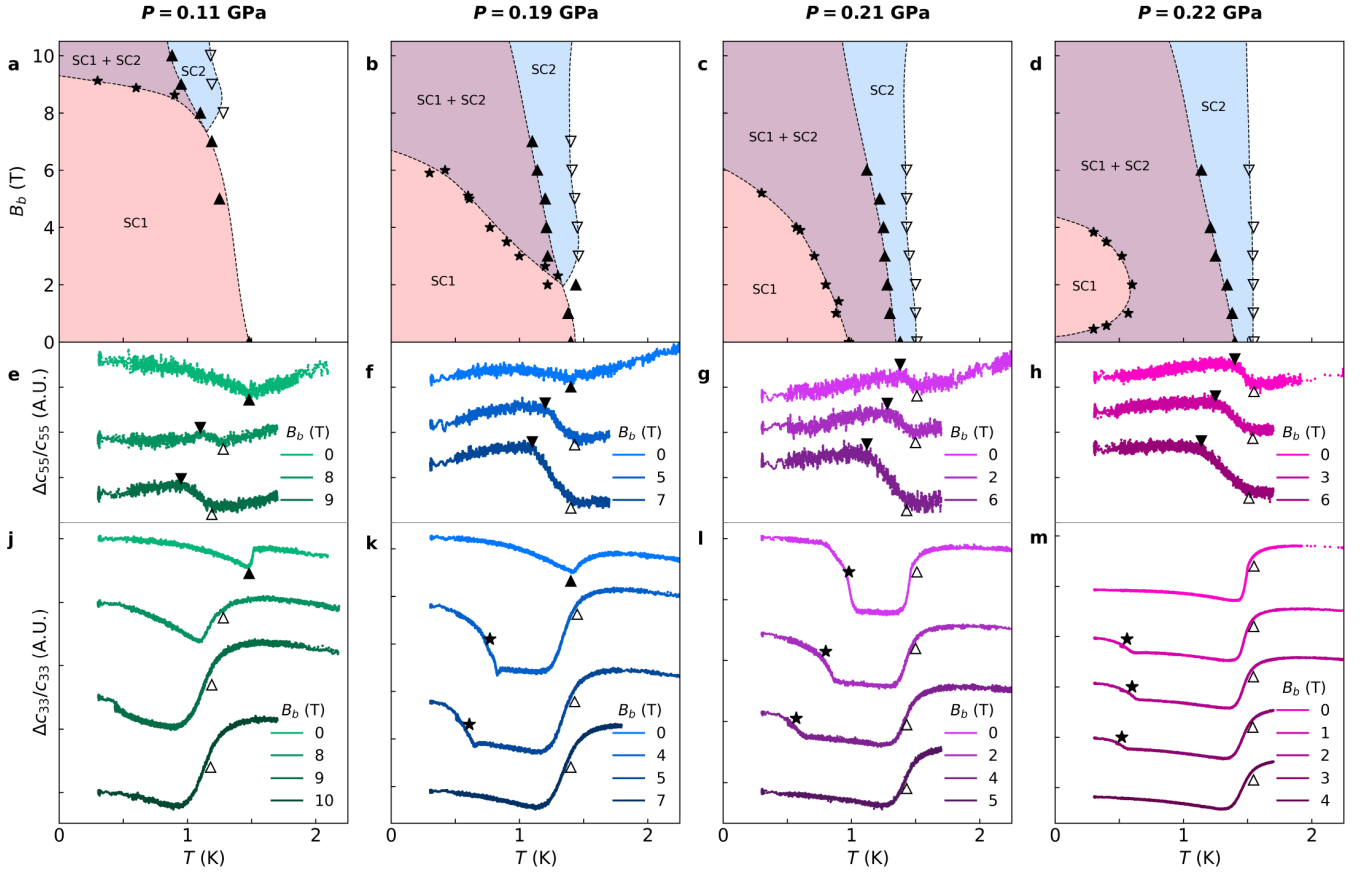


FIG. 3. **Field-temperature phase diagrams of UTe_2 at fixed pressure.** Corresponding c_{55} and c_{33} data are shown directly below. T_{c1} , T_{c2} and T_{c2}^* measured in this work are represented by solid triangles, hollow triangles, and stars respectively. a-d) Phase diagrams. Regions in phase space where the SC1, SC2, and SC1+SC2 order parameters are non-zero are shaded in red, blue, and purple, respectively. e-h) c_{55} elastic modulus data. T_{c1} and T_{c2} are seen as sharp kinks in the data. j-m) c_{33} elastic modulus data. The downward jumps upon cooling correspond to T_{c1} or T_{c2} , while the upward jumps correspond to T_{c2}^* .

over a very narrow range in pressure, and we are unable to tune pressure *in-situ*. To place stronger constraints on this boundary, we measure c_{33} and c_{55} as a function of magnetic field along the b -axis and track T_{c2}^* across the full B_b - P - T phase diagram.

We construct field-temperature phase diagrams at 4 distinct pressures in the vicinity of P^* , shown in Figure 3a-d. Below each phase diagram we show selected elastic moduli versus temperature curves that are used to construct these phase diagrams—full data sets are provided in the Extended Data. Figure 3e-h shows select c_{55} curves, and Figure 3j-m shows select c_{33} curves.

As with the zero-field phase diagram shown in Figure 2, we use kinks in c_{55} and jumps in c_{33} to identify the phase boundaries: T_{c1} is indicated with solid triangles, and T_{c2} is indicated with hollow triangles. We find that the pressure-induced SC2 phase is indeed topologically connected to the field-induced phase, consistent with previous reports [10].

The new information contained in these data is the field and pressure evolution of T_{c2}^* . Similar to zero-

pressure (but broadened slightly because of the magnetic field), we find upward jumps in c_{33} upon cooling through T_{c2}^* . The magnitudes of these jumps are again similar to what we find at T_{c1} . These phase boundaries represent the transition from the mixed SC1+SC2 phase to the pure SC1 phase—to our knowledge, these phase boundaries have never been reported.

The T_{c2}^* boundary in the field-temperature phase diagram evolves rapidly with pressure. At $P = 0.11$ GPa, the tetracritical point is located near 7 tesla and 1.25 kelvin. As pressure is increased, the field value at which this tetracritical point occurs decreases rapidly, reaching zero field at P^* and providing the tetracritical point shown in Figure 2. Thus while the T_{c2}^* line is constrained by only one data point in zero magnetic field, Figure 3 tracks the T_{c2}^* line at many different points at finite magnetic field, tightly constraining the position of the T_{c2}^* line in Figure 2. Past P^* , the pure SC1 phase is “pinched off” at zero magnetic field, confined to a small pocket between 0 and 600 mK, and between 0 and 4 tesla.

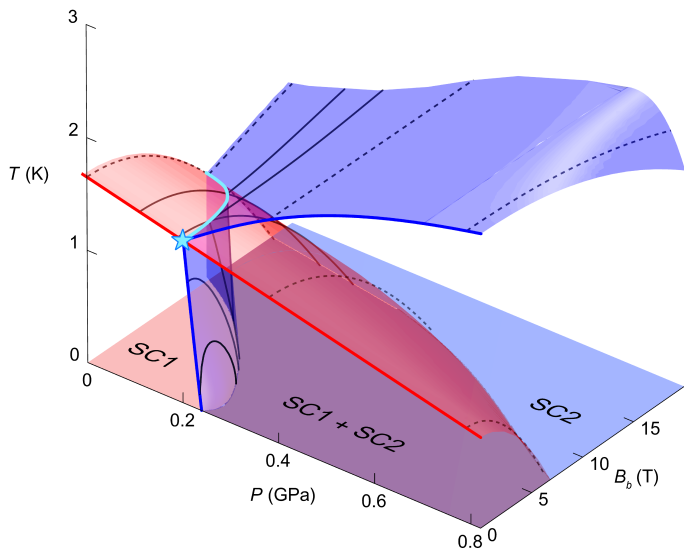


FIG. 4. **Field-Temperature-Pressure phase diagram of UTe_2 .** SC1 and SC2 phase boundaries are represented by red and blue sheets respectively. The solid red and blue lines on the $B = 0$ plane represent the zero-field phase boundary from this work (Figure 2a), while the solid black lines represent the constant-pressure phase boundaries shown in Figure 3a-d. Dashed black lines are adapted from Vasina et. al. [10]. The zero temperature ground states of the system are shown on the $T = 0$ plane. The tetracritical point in the $P - T$ plane—(P^* , T^*), indicated with a light-blue star—becomes a line of tetracritical points in B_b - P - T space, indicated by the light-blue line. This line terminates at 12 tesla and 1 kelvin at ambient pressure. Between 12 and 18 tesla, the SC1+SC2 state exists at ambient pressure.

The full magnetic field-pressure-temperature phase diagram

The phase diagrams we have constructed in b -axis magnetic field, pressure, and temperature, can be combined into a three-dimensional B_b - P - T diagram, shown in Figure 4 (details of how this phase diagram is constructed are given in the caption). The two component state SC1+SC2 occupies a large region of phase space extending down to zero pressure for magnetic fields $B_b > 12$ T.

ANALYSIS

Competing superconducting orders

The phase diagram shown in Figure 4 is highly unusual in that the SC2 phase boundary bends back on itself when it hits the SC1 phase boundary. This leads to

a narrow pressure range over which the SC2 order parameter is reentrant as a function of temperature. Can such an exotic phase diagram be explained within a Ginzburg Landau (GL) framework? While novel for a superconducting state, similar back-bending is observed at the intersection of antiferromagnetism (AFM) and superconductivity in the iron pnictides. There, it is explained in terms of a competition between the superconducting and AFM order parameters (OPs) [17]. In this section, we use the zero-field phase diagram to construct a phenomenological GL theory of two interacting superconducting OPs.

We begin with two non-interacting OPs, ψ_1 and ψ_2 , corresponding to the SC1 and SC2 states. Each independent ψ_i has a free energy $F_i = \frac{a_i}{2} |\psi_i|^2 + \frac{u_i}{4} |\psi_i|^4$. Without any interaction between them, the total free energy is simply $F = F_1 + F_2$, with a phase diagram in the form of Figure 1a — two phase boundaries crossing one another without any change in slope.

However, the experimental SC2 phase boundary changes slope (quite dramatically) when it hits the SC1 phase boundary. To account for this, we add the lowest-order, symmetry-allowed terms that couple ψ_1 and ψ_2 :

$$F = F_1 + F_2 + \frac{\gamma_1}{2} |\psi_1|^2 |\psi_2|^2 + \frac{\gamma_2}{4} (\psi_1^2 \psi_2^{*2} + h.c.) \quad (2)$$

Here, γ_1 couples the two OP magnitudes, while γ_2 locks the relative phase of the two complex OPs. The sign of γ_2 determines whether the SC1+SC2 breaks time reversal ($\gamma_2 > 0$) or not ($\gamma_2 < 0$). The competition of the two phases is governed in either case by the parameter $\gamma \equiv \gamma_1 - |\gamma_2|$.

There are three key features of the experimental phase diagram that constrain the GL theory: (i) the phase lines meet at a tetracritical point; (ii) the slope of T_{c1} versus pressure is almost unaffected by the intersection with T_{c2} ; and (iii) the new SC1 \leftrightarrow SC1+SC2 phase boundary bends backwards. These three observations give rise to the following three constraints:

Observation	Constraint
Tetracrit. point	$0 < \gamma < \sqrt{u_1 u_2}$
T_{c1} unaffected	$\gamma \ll u_2$
Back bending	$\gamma > u_1$,

where the u_i are the quartic coefficients of the uncoupled theory and we use a convention for the quadratic coefficients a_i discussed in the Methods section.

These constraints naturally explain the observed hierarchy of specific jumps at the various transitions. Specifically, they explain why the jump at the upper T_{c2} transition is small compared to the jump at T_{c1} —a fact that led to various alternative explanations of the phase diagram. First, the ratio of the specific heat jumps at the transitions from the normal metal to the single-component states is given by the inverse ratio of the quartic interactions, i.e. $(\Delta C/T|_{T_{c1}})/(\Delta C/T|_{T_{c2}}) = u_2/u_1$. Eq. (3) requires this ratio to be large—the jump at T_{c1} should

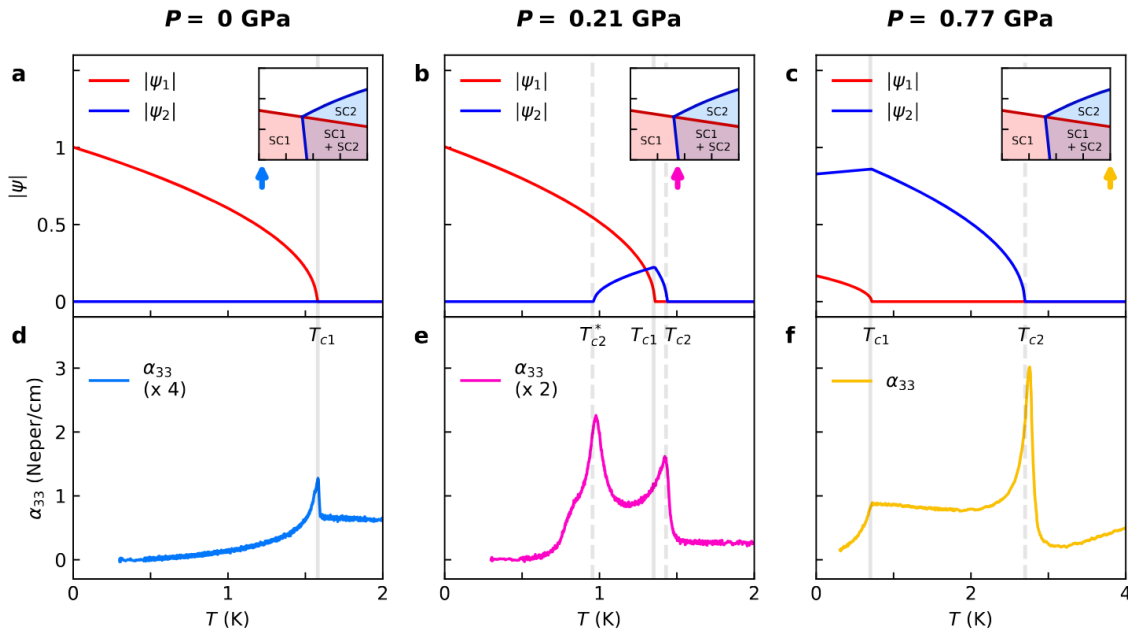


FIG. 5. **Order parameter competition in UTe₂.** a-c) The order parameters magnitudes for the SC1 ($|\psi_1|$) and SC2 ($|\psi_2|$) states versus temperature at different pressures. T_{c1} is indicated by a solid gray line, while T_{c2} and T_{c2}^* are indicated by dashed gray lines. Insets show where each pressure lies on the phase diagram of Figure 2a. d-f) Ultrasonic attenuation α_{33} versus temperature at different pressures. We find an parameter relaxation peak as the sample enters the SC1 state at 0 GPa, and as the sample enters and exits the SC2 state at 0.21 GPa. At 0.77 GPa, anomalously large phase fluctuations [13] cause the ultrasonic attenuation inside the SC2 state to be larger than the normal state value. α_{33} decreases as the SC1 order parameter grows and suppresses phase fluctuations below T_{c1} .

be much larger than the jump at T_{c2} —which is fully consistent with the data of Refs.[7, 8, 10]. Second, the jump at the transition from SC2 to SC2+SC1 is given by $\Delta C/T|_{T_{c1}} = \Delta C/T|_{T_{c2}} \times \frac{(u_2 - \gamma)^2}{u_1 u_2 - \gamma^2}$. The above conditions require that the jump at T_{c1} to the SC1+SC2 phase is much larger than the jump at T_{c2} to the SC2 phase, which is again in full agreement with the data[7, 8, 10]. Finally, a consequence of the back bending is that the jump at T_{c2}^* is negative: $\Delta C/T|_{T_{c2}^*} = -\Delta C/T|_{T_{c1}} \times \frac{(u_1 - \gamma)^2}{u_1 u_2 - \gamma^2}$, as discussed out earlier. Full calculations are given in the Methods.

With the GL parameters constrained by the phase diagram, the competition between SC1 and SC2 can be visualized by plotting $|\psi_1|$ and $|\psi_2|$ as a function of temperature alongside the α_{33} sound attenuation coefficient. Sound attenuation in a metal at low temperatures is dominated by the conduction electrons—in the superconducting state, the sound attenuation generally decreases as the normal quasiparticles are gapped out (see Kamat et al. [13] for further discussion). Figure 5a illustrate this at ambient pressure: the sound attenuation decreases to zero as $|\psi_1|$ grows with decreasing temperature. Near T_{c1} , we find an order parameter fluctuation peak in α_{33} that is indicative of a sign-changing gap, as discussed in Kamat et al. [13] and seen in other heavy fermion superconductors [18, 19].

Competition between the two order parameters is clearly visible at $P = 0.21$ GPa—slightly greater than P^* —as shown in Figure 5b. The growth of $|\psi_2|$ below T_{c2} is sharply curtailed by the appearance of $|\psi_1|$ at T_{c1} . Below T_{c1} ψ_1 grows unimpeded, while ψ_2 is suppressed. This suppression is complete by T_{c2}^* . The ultrasonic attenuation α_{33} , shown in Figure 5e, shows attenuation peaks at both entrance to and exit out of the SC2 phase consistent with SC2 also having a sign-changing gap.

At the highest pressure— $P = 0.77$ GPa— $|\psi_2|$ has a much broader region to establish itself before being truncated by the appearance of $|\psi_1|$ (Figure 5c). The sound attenuation is most dramatic here: below the fluctuation peak at T_{c2} , the sound attenuation remains *larger* than its normal state value all the way down to T_{c1} , at which point it drops toward zero. We attribute this excess sound attenuation to the anomalously low phase stiffness of the SC2 phase [13]—an attribution also consistent with the constraints in Equation 3. Within our GL analysis, we show that the quartic coupling term $e(\psi_1^2 \psi_2^{*2} + h.c.)$ locks the relative phase of the two OPs, allowing the SC2 state to gain phase stiffness from the SC1 state, suppressing the phase fluctuations that produce the anomalous sound attenuation for $T_{c1} < T < T_{c2}$ (see Methods).

DISCUSSION

Our discovery of the phase transition line at T_{c2}^* establishes that: 1) $(P^*, T^*) \approx (0.20 \text{ GPa}, 1.4 \text{ K})$ is a tetracritical point; 2) this extends to a tetracritical line in the B - P - T phase diagram; 3) the SC2 phase is strongly influenced by the SC1 phase, but not the other way around; and 4) there is a region of the B - P - T phase diagram with multi-component superconductivity. The obvious question is whether this multi-component state is time reversal symmetry breaking and possibly topological.

Whether or not the SC1+SC2 state breaks time reversal depends on the sign of γ_2 in Eq. (2). A negative value implies a trivial combination of the two OPs with the same phase, while a positive value implies that relative phase between the two OPs is $\pi/2$, leading to a chiral $\psi_1 + i\psi_2$ state that breaks time reversal symmetry (TRS). As we discuss in the SM, if the spin structure of the two triplet states in momentum space is similar, we find that $\gamma_2 > 0$ and that time-reversal symmetry breaking is favoured in SC1+SC2.

While our measurements cannot directly determine whether or not the SC1+SC2 phase breaks time reversal, the fact that the SC1+SC2 phase expands with increasing magnetic field (as we show in Figure 4) suggests a time-reversal symmetry breaking multi-component state, or perhaps a pairing interaction for the SC2 phase that is enhanced by magnetic field.

Finally, we comment on the microscopic implications of the hierarchy in the quartic couplings of the GL parameters, $u_1 < \gamma \ll u_2$. As we show in the Methods, this hierarchy has rather clear consequences for the electronic states that form the Cooper pairs. In particular, such a pronounced separation of coupling strengths can arise only if the orbitals that contribute significantly to the large density of states enter more prominently into the pair wave function in SC2 than in SC1. This insight therefore imposes a stringent constraint on any microscopic theory of the pairing mechanism in UTe₂

ACKNOWLEDGMENTS

Research at Cornell was supported by the Department of Energy, Office of Basic Energy Sciences Award No. DE-SC-0026003 (ultrasound measurements and data analysis). Research at the University of Maryland was supported by the Gordon and Betty Moore Foundation's EPiQS Initiative Grant No. GBMF9071 (materials synthesis), the Department of Energy, Office of Basic Energy Sciences Award No. DE-SC-0019154 (sample characterization), the NIST Center for Neutron Research, and the Maryland Quantum Materials Center. Theory work was supported by the German Research Foundation TRR 288-422213477 ELASTO-Q-MAT, A07 (A.D.K. and J.S.) and grant SFI-MPS- NFS-00006741-05 from the Simons Foundation (J.S.).

-
- [1] C. Kallin, Chiral p-wave order in Sr₂ RuO₄, [Reports on Progress in Physics](#) **75**, 042501 (2012).
 - [2] D. Vollhardt and P. Wolfe, [The Superfluid Phases of Helium 3](#) (Courier Corporation, 2013).
 - [3] M. Sigrist and K. Ueda, Phenomenological theory of unconventional superconductivity, [Reviews of Modern Physics](#) **63**, 239 (1991).
 - [4] M. Sato and Y. Ando, Topological superconductors: a review, [Reports on Progress in Physics](#) **80**, 076501 (2017).
 - [5] F. Theuss, A. Shragai, G. Grissonnanche, I. M. Hayes, S. R. Saha, Y. S. Eo, A. Suarez, T. Shishidou, N. P. Butch, J. Paglione, and B. J. Ramshaw, Single-component superconductivity in UTe₂ at ambient pressure, [Nature Physics](#) **20**, 1124 (2024).
 - [6] P. F. S. Rosa, A. Weiland, S. S. Fender, B. L. Scott, F. Ronning, J. D. Thompson, E. D. Bauer, and S. M. Thomas, Single thermodynamic transition at 2 K in superconducting UTe₂ single crystals, [Communications Materials](#) **3**, 33 (2022).
 - [7] D. Braithwaite, M. Vališka, G. Knebel, G. Lapertot, J.-P. Brison, A. Pourret, M. E. Zhitomirsky, J. Flouquet, F. Honda, and D. Aoki, Multiple superconducting phases in a nearly ferromagnetic system, [Communications Physics](#) **2**, 147 (2019).
 - [8] S. M. Thomas, F. B. Santos, M. H. Christensen, T. Asaba, F. Ronning, J. D. Thompson, E. D. Bauer, R. M. Fernandes, G. Fabbri, and P. F. S. Rosa, Evidence for a pressure-induced antiferromagnetic quantum critical point in intermediate-valence UTe₂, [Science Advances](#) **6**, eabc8709 (2020).
 - [9] Z. Wu, J. Chen, T. I. Weinberger, A. Cabala, V. Sechovský, M. Vališka, P. L. Alireza, A. G. Eaton, and F. M. Grosche, Magnetic Signatures of Pressure-Induced Multicomponent Superconductivity in ut₂, [Physical Review Letters](#) **134**, 236501 (2025).
 - [10] T. Vasina, D. Aoki, A. Miyake, G. Seyfarth, A. Pourret, C. Marcenat, M. Amano Patino, G. Lapertot, J. Flouquet, J.-P. Brison, D. Braithwaite, and G. Knebel, Connecting High-Field and High-Pressure Superconductivity in ut₂, [Physical Review Letters](#) **134**, 096501 (2025).

- [11] S. K. Yip, T. Li, and P. Kumar, Thermodynamic considerations and the phase diagram of superconducting UPt_3 , *Physical Review B* **43**, 2742 (1991).
- [12] S. Ghosh, A. Shekhter, F. Jerzembeck, N. Kikugawa, D. A. Sokolov, M. Brando, A. P. Mackenzie, C. W. Hicks, and B. J. Ramshaw, Thermodynamic evidence for a two-component superconducting order parameter in Sr_2RuO_4 , *Nature Physics* **17**, 199 (2021).
- [13] S. Kamat, J. Dans, S. Saha, D. F. Agterberg, J. Paglione, and B. J. Ramshaw, Vanishing Phase Stiffness and Fluctuation-Dominated Superconductivity: Evidence for Inter-Band Pairing in UTe_2 [10.48550/arXiv.2601.09138](https://arxiv.org/abs/10.48550/arXiv.2601.09138) (2026), *Under Review*.
- [14] H. B. Callen, *Thermodynamics* (John Wiley & Sons, 1991).
- [15] M. Tinkham, *Introduction to Superconductivity* (Courier Corporation, 2004).
- [16] W. Rehwald, The study of structural phase transitions by means of ultrasonic experiments, *Advances in Physics* **22**, 721 (1973).
- [17] R. M. Fernandes and J. Schmalian, Competing order and nature of the pairing state in the iron pnictides, *Physical Review B* **82**, 014521 (2010).
- [18] D. J. Bishop, C. M. Varma, B. Batlogg, E. Bucher, Z. Fisk, and J. L. Smith, Ultrasonic Attenuation in UPt_3 , *Physical Review Letters* **53**, 1009 (1984).
- [19] B. Batlogg, D. J. Bishop, E. Bucher, B. Golding, C. M. Varma, Z. Fisk, J. L. Smith, and H. R. Ott, Ultrasound studies of the heavy fermion superconductors UPt_3 , UBe_{13} and $(\text{U}, \text{Th})\text{Be}_{13}$, *Physica B+C* **135**, 23 (1985).